A new etching environment (FeF_3/HCl) for the synthesis of two-dimensional titanium carbide MXenes: a route towards selective reactivity vs. water

X. Wang, C. Garnero, G. Rochard, D. Magne, Sophie Morisset, S. Hurand, Patrick Chartier, J. Rousseau, Thierry Cabioc'H, Christophe Coutanceau, et al.

▶ **To cite this version:**

X. Wang, C. Garnero, G. Rochard, D. Magne, Sophie Morisset, et al.. A new etching environment (FeF_3/HCl) for the synthesis of two-dimensional titanium carbide MXenes: a route towards selective reactivity vs. water. Journal of Materials Chemistry A, 2017, 5 (41), pp.22012 - 22023. 10.1039/C7TA01082F . hal-01915184

HAL Id: hal-01915184
https://hal.science/hal-01915184v1

Submitted on 29 Aug 2024

HAL is a multi-disciplinary open access archive for the deposit and dissemination of scientific research documents, whether they are published or not. The documents may come from teaching and research institutions in France or abroad, or from public or private research centers.

L'archive ouverte pluridisciplinaire **HAL**, est destinée au dépôt et à la diffusion de documents scientifiques de niveau recherche, publiés ou non, émanant des établissements d'enseignement et de recherche français ou étrangers, des laboratoires publics ou privés.

Please do not adjust margins

Journal Name

ARTICLE

New etching environment (FeF_3/HCl) for the synthesis of two-dimensional titanium carbide MXenes: a route towards selective reactivity vs water

Received 00th January 20xx,
Accepted 00th January 20xx

DOI: 10.1039/x0xx00000x

www.rsc.org/

X. Wang,[a,b] C. Garnero,[a,b] G. Rochard,[a] D. Magne,[b] S. Morisset,[a] S. Hurand,[b] P. Chartier,[b] J. Rousseau,[a] T. Cabioc'h,[b] C. Coutanceau,[a] V. Mauchamp*[b] and S. Célérier.*[a]

The synthesis of $Ti_3C_2T_x$ (and Ti_2CT_x alike) MXenes is performed with a new etching environment (FeF_3/HCl). Significant differences in terms of surface functionalization (including the insertion of iron cations between the MXenes sheets), morphology, nature of impurities, water intercalation and reactivity are obtained in comparison with samples prepared with the conventional HF or LiF/HCl etching methods. In particular, the new synthesis method allows modifying the reactivity of Ti_3C_2 vs water with improved selectivity towards the formation of TiO_2 anatase nanoparticles on the MXene sheets whereas rutile TiO_2 nanoparticles are favoured with the LiF/HCl method. The role of the Fe^{n+} and Al^{3+} cations inherent to this synthesis process on the inhibition of the anatase to rutile transformation is shown to be a key parameter. In addition, the MXene oxidation rate in water is also increased when the material is prepared with FeF_3/HCl compared to the LiF/HCl method owing to the surface modification of the MXene during the etching step. This oxidation rate can easely be tuned by the duration of immersion. This work expands the number of etching methods to form MXenes while offering new opportunities in the rationalized design of MXene-TiO_2 nanocomposite structures for future applications.

1 Introduction

A new family of two-dimentional (2D) materials consisting in few atomic layers thick transition metal carbide or carbonitride sheets with chemical composition $M_{n+1}X_n$ (M : d-block transition metal, X : C or N atoms) known as MXene, has been recently discovered.[1,2] These materials are produced by the selective etching of the A element layers (mostly from groups 13 and 14 of the periodic table) from the $M_{n+1}AX_n$ phases, which is a 70-members family of layered, hexagonal early-transition-metal carbides and nitrides.[3] The MXene family is thus expected to be particularly large. Beyond the exciting fundamental scientific aspect for developing 2D systems with tunable chemical compositions, the interest for MXenes is currently particularly high since these materials show great potentials in several applications such as supercapacitors,[4,5] lithium[6,7] or non-lithium ion batteries,[8] fuel cells,[9] electrolytic/solar water splitting,[10] catalysis,[11,12] hydrogen storage,[13] biosensor,[14] photocatalysis,[15] optical transparent thin films[16] and separation or purification.[17-19] The properties and applications of these materials have been recently reviewed.[20-23]

To date, the majority of MXenes have been synthesized by etching the corresponding $M_{n+1}AX_n$ phase in concentrated hydrofluoric acid (HF).[20,21] Doing so, $M_{n+1}X_n$ weakly interacting sheets are obtained, these sheets being mainly functionalized with OH, O and/or F surface termination groups (labeled T) formed during the synthesis by reaction with the environment (H_2O and HF) and leading to the following formula: $M_{n+1}X_nT_x$.[24,25] The T-groups play a key role in the MXenes properties since, depending on their chemical nature and location on the MXene surface, they can modify the energy storage capacities,[8,26] induce magnetism,[27] modify the surface plasmon resonance[28] or transport properties[29] among others. The control of the location, composition and densities of the T-groups on the MXene surface, and the MXene functionalization processes in general, is clearly an important step in the rationalized design of these materials. In this context, the control of the etching process is obviously one of the most appropriate ways to do so.

Recently, two alternative methods to the HF process were proposed. Halim et al[30] used ammonium fluoride (NH_4HF_2) as etching agent to produce $Ti_3C_2T_x$ films. From these milder conditions, etching of Al and intercalation of NH_3 and NH_4^+ occur simultaneously. The use of LiF in HCl (or LiCl in HF) solution has also been reported by Ghidiu et al.[31,32] to produce $Ti_3C_2T_x$ leading to the formation of a clay-like material, which facilitates the processing of free-standing films. Intercalation of water and lithium has been reported using this method. Moreover, the possibility to replace LiF by NaF, KF, CsF, tetrabutylammonium fluoride or CaF_2, showing similar etching behavior, is also proposed by Ghidiu et al.[31] Beyond avoiding the handling of hazardous concentrated HF environment, these

[a] Institut de Chimie des Milieux et Matériaux de Poitiers (IC2MP), Université de Poitiers, CNRS, F-86073 Poitiers, France. E-mail : stephane.celerier@univ-poitiers.fr
[b] Institut Pprime, UPR 3346 CNRS – Université de Poitiers – ISAE-ENSMA, BP 30179, 86962 Futuroscope-Chasseneuil Cedex, France, E-mail : vincent.mauchamp@univ-poitiers.fr
Electronic Supplementary Information (ESI) available: See DOI: 10.1039/x0xx00000x

Please do not adjust margins

Please do not adjust margins

promising processes could lead to the potential tuning of the MXene surface composition, texture and delamination and thus to provide new opportunities in terms of applications for this family of 2D materials. For example, Liu et al.[33] point out the possibility to tune the methane adsorptive properties of the MXenes as a function of the etching agent (LiF, NaF, KF or NH4F in HCl), the most promising results being obtained with LiF.

The physicochemical properties of MXenes can be further improved when used in composite materials.[23] In this context, the controlled oxidation of Ti-based structures, leading to the formation of TiO_2 (rutile or anatase) nanoparticles (Nps) on the MXene surface, offers many opportunities in terms of application for lithium ion batteries,[34] supercapacitors,[35] photocatalysis[36] or sensors.[37] Controlling the rate of the oxide formation and of its anatase or rutile structure becomes then another key element for the rational design of these systems. Anatase is the stable polymorph structure in the case of Nps with sizes below ~15 nm whereas rutile becomes more stable for larger Nps.[38] Knowing the high reactivity of MXenes vs cations and the crucial role of many cations on the anatase-to-rutile transformation (AR-T),[39] our goal is to develop a new single step synthesis method allowing to prepare MXenes with controlled surface chemistry and cation intercalation into the MXenes. Li^+ is known to promote the AR-T, therefore we have focused on the insertion of Fe^{n+} ions which have been shown to inhibit this transformation in weakly loaded systems.[40]

For this purpose, we propose a new etching method for the production of $Ti_{n+1}C_nT_x$ from $Ti_{n+1}AlC_n$ (n = 1 or 2), by far the most studied MXenes to date, using a mixture of iron fluoride (FeF_3) and hydrochloric acid (HCl). The aims of this work are: (i) to replace the lithium due to its limitation as a natural resource[31] by the fourth most abundant element in earth crust, i.e. iron, (ii) to insert iron atoms between the MXene layers in order to modify their surface properties and particularly their reactivity towards water, a chemical environment widely used for many of the above-mentioned applications, (iii) to control the partial oxidation of the MXene by tuning the AR-T with the inserted cations (iv) to modify the chemical compositions and the textural properties of the MXenes in comparison with those issued from the classical HF treatment and LiF/HCl method and (v) to expand the numbers of etching methods which is desirable for future explorations in the MXene domain. This work aims to highlight the crucial role of the selected etching environment on the surface properties of the MXenes.

2 Experimental

2.1 Synthesis of materials

- Synthesis of Ti_3C_2 by HF exfoliation (Ti_3C_2-HF)

21 mL of aqueous HF (Sigma-Aldrich, ≥ 48%) were introduced in a plastic vessel containing 2 g of Ti_3AlC_2 (see ESI, section I, for the MAX synthesis) with initial particles sizes lower than 25 μm obtained after sieving. The exfoliation of aluminum was performed at room temperature for 24h. Rapid formation of bubbles (hydrogen evolution) was observed and the reaction was very exothermic. The resulting suspension was filtered using a vacuum-assisted filtration device (PVDF membrane, 0.22 μm pore size) and washed several times with deionized water. The obtained powders were dried at 80°C for 24h.

- Synthesis of Ti_3C_2 by FeF_3/HCl or LiF/HCl exfoliation (Ti_3C_2-Fe and Ti_3C_2-Li)

2 g of $FeF_3.3H_2O$ (Aldrich) (or 1 g of LiF from Aldrich) were added to 20 mL of HCl 6M (7M for LiF/HCl etching process), prepared from HCl 37% (Sigma-Aldrich) and stirred during 30 min. Then, 1.5 g of Ti_3AlC_2 (particle sizes ≤ 25 μm) were progressively introduced in the solution to avoid initial overheating. The mixture was heated at 60°C for 50 h (90 h for LiF/HCl etching process). Then the suspension was filtered, washed and dried as described for the HF exfoliation method. The method used with LiF/HCl is partly based on the work of Ghidiu et al.[31] For specific experiments, The influence of an acid (HCl) washing step by centrifugation was also studied (see ESI – section VI).

- Synthesis of Ti_2C by FeF_3/HCl exfoliation (Ti_2C-Fe)

The synthesis procedure is similar to that of Ti_3C_2-Fe except for the duration of the exfoliation (25 h instead of 50 h) and the nature of the MAX phase precursor: Ti_2AlC (particle sizes ≤ 25 μm).

2.2 Reactivity vs water

0.8 g of Ti_3C_2 were added to 350 mL of deionized water (w) and stirred at room temperature during 50 or 168 h (1 week). The samples are referred as to Ti_3C_2-M-w50h and Ti_3C_2-M-w168h with M = Fe, Li or HF depending on the exfoliation process used to form the MXene phase. For the sample prepared with FeF_3/HCl, the influence of the duration of immersion in water was also studied from 1h to 168h. In a similar way, 0.8 g of Ti_3C_2 were added to 350 mL of deaerated water (d) during 168 h: the samples are referred as Ti_3C_2-M-d (with M = Fe, Li or HF). The powders were then filtered, washed and dried as described for the HF exfoliation method.

2.3 Characterization

XRD analysis of the MXene powders were carried out with a PANalytical EMPYREAN powder diffractometer using CuK_α radiation source (K_{α_1} = 1.5406 Å and K_{α_2} = 1.5444 Å). XRD patterns were collected between 5 and 50° with a 0.07° step and 420 s dwell time at each step. The identification of $TiOF_2$, Ti_3AlC_2, Ti_2AlC, TiO_2 anatase and TiO_2 rutile phases was performed with the HighScorePlus software (PANalytical©) and by comparison with the ICDD database reference files. Phase identification of MXene from the XRD patterns is based from works in the literature.[1,31,32]

Specific surface area measurements were performed using nitrogen adsorption at -196°C with a TRISTAR 3000 gas adsorption system. Prior N_2 adsorption, the powder samples were degassed under secondary vacuum for 12 h at 80°C. The BET equation was used to calculate the specific surface area of the samples (S_{BET} in $m^2\ g^{-1}$).

The aluminum, titanium and iron contents of the different Ti_3C_2 were determined by Inductively Coupled Plasma-Optical Emission Spectrometry (ICP-OES) using a PerkinElmer Optima 2000DV instrument. The determined contents of each element were rationalized to 3 titanium atoms.

The morphology of the MXene powders was studied using a field emission gun scanning electron microscope (FEG-SEM) 7001F from JEOL. This microscope is equipped with an Energy Dispersive X-ray Spectrometer (EDS) from OXFORD (with Aztec software) allowing the

 This journal is © The Royal Society of Chemistry 20xx

Please do not adjust margins

Please do not adjust margins

determination of the O, F, Al, Ti, and C contents. Due to the nature of the sample support (double-face adhesive carbon), the carbon content was not taken into account. The determined contents of each element were rationalized to 3 titanium atoms.

The crystallography and site-projected electronic structure of the different samples were investigated on the nanometer scale using a combination of transmission electron microscopy (TEM) and electron energy-loss spectroscopy (EELS). EELS has indeed recently been demonstrated to be a powerful tool for the investigation of the MXenes electronic structure (including surface groups) at the single nano-object level thereby avoiding the critical question of impurities.[16,25] TEM-EELS experiments were conducted on a JEOL 2200-FS microscope equipped with an in-column omega filter and operated at 200 kV. The energy resolution determined from the zero-loss peak full width at half maximum was 0.8 eV. Data were processed using a standard procedure: the core-edges (*i.e.* the C K-edge around 283 eV and the F K-edge around 685 eV) were extracted from the background using a power law and were deconvolved from multiple scattering using the Fourier-ratio method.[42]

EELS being mainly sensitive to the volume of the sample at the TEM scale, surface sensitive electronic structure characterizations were, in a complementary way, performed using X-Ray photoelectron spectroscopy (XPS). XPS spectra were collected with a Kratos Axis Ultra DLD spectrometer using a monochromatic Al K_α source (10 mA, 15 kV). Operating pressure for analysis was 9 x 10^{-8} Pascal. When required, charge compensation was achieved by using a charge neutraliser. High-resolution spectra were recorded using an analysis area of 300 µm x 700 µm and 40 eV pass energy. This pass energy corresponds to Ag $3d_{5/2}$ FWHM of 0.55 eV. Data were acquired with 0.1 eV steps. Samples were pressed onto a double-sided adhesive tape. Spectral processing were analysed with CasaXPS software (version 2.3.17 dev6.3a) and peak fitting were performed with Gaussian-Lorentzian profiles, an asymmetric shape was added for Ti2p (Titanium carbide).

Raman spectra were also used to characterize MXenes. Spectra were collected through a HORIBA Jobin Yvon HR800 confocal Raman microscope with a CCD detector. Representative spectra were acquired at ambient conditions using an excitation wavelength of 532 nm.

3 Results and discussion

3.1 MXene synthesis

The X-ray diffraction (XRD) patterns of the samples obtained for each etching environment after drying at 80°C are compared with the XRD pattern of the initial Ti_3AlC_2 in Fig. 1. Whatever the etching environment, the initial MAX phase disappears entirely, as evidenced by the absence of the corresponding sharp diffraction peaks at 2θ of 9.54° and 19.18°, attesting the total etching of the aluminum and the formation of the MXene phase. A drastic crystallinity loss, characterized by a broadening of the XRD peaks and the decrease of their intensity, is also evidenced. The XRD pattern of Ti_3C_2-HF is similar to those reported previously in the literature and prepared under the same conditions.[1] The (002) peak of the initial MAX phase is shifted towards lower angles (9.00°) indicating a higher c parameter value (19.62 Å) compared to the initial MAX phase (9.54° - c = 18.52 Å). This is due to the presence of terminal groups (T = O, OH and/or F) which increases the intersheet distance.[1] On this sample, $TiOF_2$ is also evidenced as a secondary phase. This phase, already observed sometimes with HF,[43] is probably formed due to the harsh environment (aqueous concentrated HF). For Ti_3C_2-Fe and Ti_3C_2-Li, this secondary phase is not observed, these media being less aggressive. Nevertheless, $AlF_3.3H_2O$ is observed on Ti_3C_2-Fe. To remove this phase, a washing step into deaerated water is necessary (see experimental section). At this point, according to XRD measurements (Fig. 1) the washed sample (Ti_3C_2-Fe-d) is a pure MXene phase and according to ICP-OES analysis (table 1) a very low amount of aluminum (Ti/Al atomic ratio: 3/0.03) remains on the sample, confirming the removal of aluminum fluoride (the Ti/Al atomic ratio before washing was 3/0.51). As indicated in table 1, aluminum is also detected by ICP-OES in Ti_3C_2-HF and Ti_3C_2-Li samples before the washing step while no crystallized aluminum phase is evidenced by XRD. This shows that the three methods lead to different behavior concerning the aluminum etching as discussed below. Interestingly, the (002) peak of Ti_3C_2-Fe shifts down to 8.01°, which corresponds to a c parameter value of 22.05 Å higher than that of Ti_3C_2-HF (c = 19.62 Å). This shift towards lower 2θ values is also observed with Ti_3C_2-Li (7.67° - c = 23.02 Å).

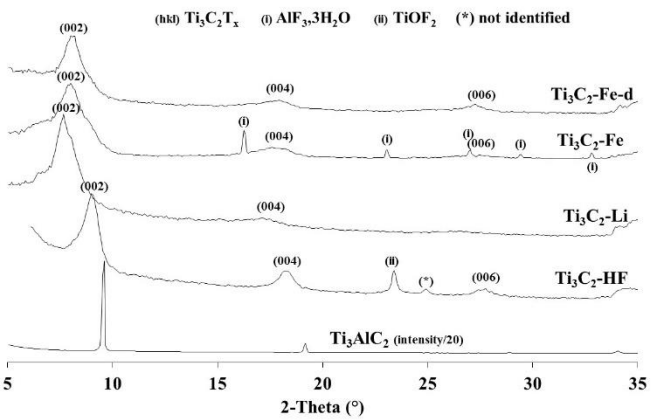

Fig. 1 XRD patterns of as-prepared Ti_3AlC_2, Ti_3C_2-HF, Ti_3C_2-Li, Ti_3C_2-Fe and Ti_3C_2-Fe-d.

Note that before drying at 80°C, the c parameter of the Ti_3C_2-Fe sample is increased up to 27.2 Å with a narrower and more intense (002) peak (Fig. 2). On the contrary, the drying step has no effect on the XRD pattern of the HF-treated sample, the structure of this MXene being less sensitive to a wet environment as observed by Ghidiu et al.[32] This phenomenon was also observed with Ti_3C_2 prepared from LiF/HCl etching treatment in agreement with the results in the work of Ghidiu et al.[31] In the case of the sample treated by LiF/HCl, the important shift of the (002) peak position towards low 2θ values is explained by the presence of water layers and insertion of cations (Li^+) in between the MXene layers.[32] In the case of the Ti_3C_2-Fe sample, ICP-OES analyses evidence the presence of iron (Table 1) in the structure. Fe was also detected by EDS (Fig. S5 – section IV of ESI) with an average amount close to 0.08 for 3 Ti, the distribution per grain being inhomogeneous (between 0 to 0.2). The obtained value is close to the value estimated by ICP. The presence

Please do not adjust margins

Please do not adjust margins

of Fe atoms within the Ti_3C_2 stacked layers is confirmed by electron energy-loss spectroscopy (EELS) as discussed later in the text. The presence of one or more water layers between the MXene layers stabilized by cations (Fe^{n+}) like in clay materials is the likely reason for the increase of the c parameter, the number of water layers depending of the drying conditions.[32] As proposed by Ghidiu et al.[32] a very few amount of cations is sufficient to stabilize the water layers (0.18 Na^+ for 3 Ti or 0.08 Mg^{2+} for 3 Ti). Moreover, the charge of the iron cation (n = 2 or 3) being higher than that of sodium cation, it is likely that a lower iron amount is needed to compensate the charge of the MXene surface and to stabilize the water layers between the $Ti_3C_2T_x$ layers. Moreover, depending on drying conditions, several (002) reflection peaks below 10° (Fig. S1 – section II of ESI) can be observed, indicating the coexistence of structures having contrasted layer-to-layer distances.[32,44] Finally, the higher crystallization state for the sample before drying can be explained by a regular distance between the MXene layers thanks to the stabilization of H_2O layers contrary to the dried samples where H_2O molecules are randomly distributed in the structure due to the inhomogeneous removal of water layers during the drying process.[32,45] To our knowledge, this is the first report of H_2O layers stabilization into MXene with iron cations. Interestingly, Co-intercalated MXenes were also prepared in our lab by replacing iron fluoride by cobalt fluoride during the etching process showing the generality of the proposed approach for the insertion of other transition metals by a one-pot synthesis.

The 2D-like morphology of the Ti_3C_2-HF, Ti_3C_2-Li and Ti_3C_2-Fe samples is evidenced by Scanning Electron Microscopy (SEM): Ti_3C_2-HF is composed of sheets formed by Ti_3C_2 multi-layers with larger intersheet gaps compared to Ti_3C_2-Fe and Ti_3C_2-Li (Fig. 3). In both latter MXenes, the sheets are tightly stacked as observed in the literature for MXene prepared with LiF/HCl etching agent as well as for cation-intercalated MXenes.[31,45] The harsh HF environment probably leads to more defects and thus to well separated sheets. On the contrary, the milder conditions with FeF_3/HCl and LiF/HCl environments and the presence of cations/water layers strengthen the cohesion between the sheets leading to more uniform structures. This is confirmed by the lower specific surface area measured by BET (table 2) for Ti_3C_2-Li and Ti_3C_2-Fe samples (less than 3 $m^2\ g^{-1}$) in comparison with Ti_3C_2-HF (10 $m^2\ g^{-1}$).

Rod-like structures of an aluminum-rich phase are also evidenced on Ti_3C_2-Fe sample (Fig. S4 – section IV of ESI) with a composition close to 1 Al for 3 F as determined by EDS and corresponding to aluminum fluoride. These kinds of structures disappear after washing (Ti_3C_2-Fe-d) confirming XRD and ICP-OES analyses. Moreover, no aluminum is significantly detected by EDS analyses (table 1) performed on isolated Ti_3C_2-Fe MXene grains indicating that the aluminum evidenced by ICP-OES is located on these rod-like structures. On the contrary, even if a significant amount of aluminum is detected by ICP-OES on Ti_3C_2-Li and Ti_3C_2-HF (table 1), these rod-like structures are not observed and aluminum is detected on isolated Ti_3C_2-HF and Ti_3C_2-Li grains with an average Ti/Al atomic ratio of 3/0.3 and 3/0.1 respectively, probably in the form of amorphous aluminum fluoride since no crystallized aluminum phase and no initial MAX phase are observed on XRD patterns (Fig. 1). Thus, the FeF_3/HCl etching environment is more efficient to remove aluminum impurities from the MXene grains favoring the formation of rod-like aluminum fluoride for an unknown reason at this stage of the study.

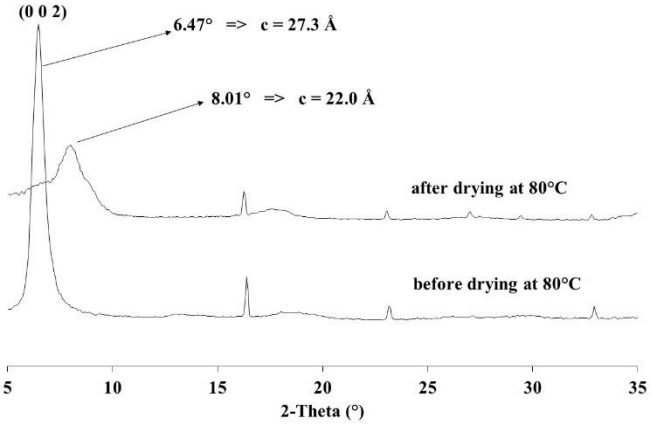

Fig. 2 XRD patterns of Ti_3C_2-Fe before and after drying at 80°C.

The 2D nanostructuration of the MXenes obtained by the new FeF_3/HCl etching method is also confirmed by Atomic Force Microscopy characterizations. As observed (Fig. S6 – section V of ESI), MXene flakes of several microns can be isolated from multilayered Ti_3C_2-Fe with a thickness of 10 to 17 nm corresponding to 7-13 layers.

Table 1 Determination of the $Ti_3C_2T_x$ samples composition by EDS and ICP-OES. The content of each element is rationalized to 3 titanium atoms.

	EDS[(a)]				ICP-OES[(b)]		
	Ti	**Al**	**F**	**O**	**Ti**	**Al**	**Fe**
Ti_3C_2-Fe	3	<0.05[(c)]	0.8	2.1	3	0.51	0.07
Ti_3C_2-Fe-d	3	<0.05[(c)]	0.7	2.8	3	0.03	0.07
Ti_3C_2-HF	3	0.3	2.6	1.5	3	0.23	-
Ti_3C_2-HF-d	3	<0.05[(c)]	1.3	2.6	3	0.02	-
Ti_3C_2-Li	3	0.1	1.1	1.2	3	0.18	-
Ti_3C_2-Li-d	3	<0.05[(c)]	0.6	2.0	3	0.03	-

(a) Average of measurements performed on isolated grains composed of several MXene sheets such as the grain on Fig. 3 (d) (local content)
(b) Global content
(c) Below the detection limit

This journal is © The Royal Society of Chemistry 20xx

Please do not adjust margins

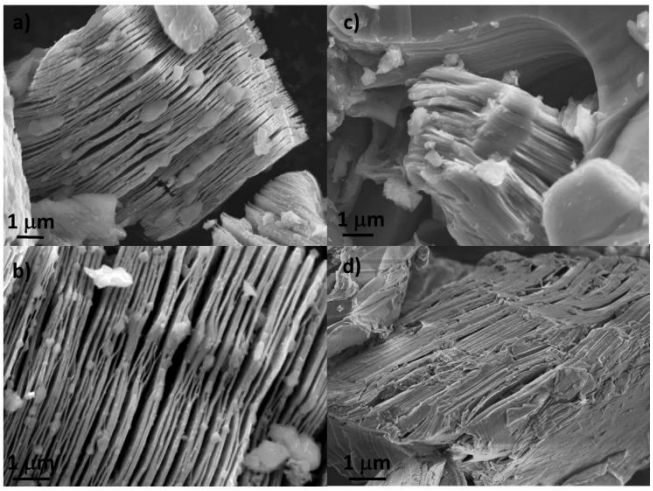

Fig. 3 Typical SEM micrographs of (a and b) Ti_3C_2-HF, (c) Ti_3C_2-Li and (d) Ti_3C_2-Fe.

Table 2 Determination of specific surface area by BET and element contents by EDS (rationalized to 3 titanium atom) of different MXenes.

	EDS			S_{BET}
	Ti	F	O	$m^2 g^{-1}$
Ti_3C_2-Fe	3	0.8	2.1	<3
Ti_3C_2-Fe-d	3	0.7	2.8	10
Ti_3C_2-Fe-w52h	3	0.7	3.9	-
Ti_3C_2-Fe-w168h	3	0.7	5.4	64
Ti_3C_2-HF	3	2.6	1.5	10
Ti_3C_2-HF-d	3	1.3	2.6	39
Ti_3C_2-HF-w168h	3	1.0	4.4	102
Ti_3C_2-Li	3	1.1	1.2	<3
Ti_3C_2-Li-d	3	0.6	2.0	8
Ti_3C_2-Li-w52h	3	0.8	2.5	-
Ti_3C_2-Li-w168h	3	0.8	4.5	27

The Raman spectra of the as-synthesized Ti_3C_2 samples with various etching environments are presented in Fig. 4. All the peaks are consistent with the vibrational modes of $Ti_3C_2T_x$ previously reported.[46-48] The absence of TiO_2 peaks indicates that the samples are not oxidized in agreement with the XRD patterns. The Raman spectra of Ti_3C_2-Li and Ti_3C_2-Fe are similar while the Raman spectra of Ti_3C_2-HF shows some different features. For Ti_3C_2-HF, an extra peak can be observed at 128 cm^{-1}: it can be attributed to a vibration mode of the Ti-F bonds.[48] Compared to Ti_3C_2-Fe and Ti_3C_2-Li, the intensity ratio between the two broad peaks around 580 and 630 cm^{-1} are reversed for Ti_3C_2-HF. Moreover, the peak observed at 730 cm^{-1} for Ti_3C_2-Fe and Ti_3C_2-Li, disappeared in favor of the peak at 700 cm^{-1}. The peaks at 700 and 730 cm^{-1} are due to a vibration mode of the Ti-F and the Ti-O bonds respectively.[48] These changes are consistent with different surface functionalizations of Ti_3C_2 due to different F ion concentrations during the etching process which influences the O/F ratio at the surface of the MXenes.[22] As discussed below, the HF etching method leads to a higher concentration of F ions in the MXene environment than the FeF_3/HCl and LiF/HCl methods. Moreover, the formation of $TiOF_2$ observed on Ti_3C_2-HF by XRD (Fig. 1) is also consistent with these Raman results.

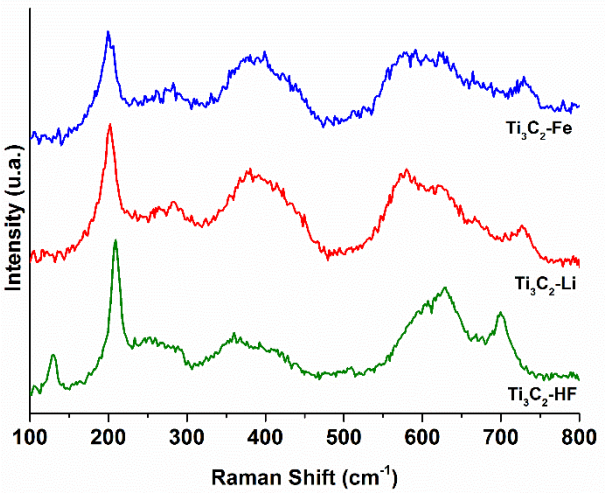

Fig. 4 Raman spectra of as prepared Ti_3C_2-HF, Ti_3C_2-Li and Ti_3C_2-Fe

The surface chemistry of the Ti_3C_2-Li and Ti_3C_2-Fe samples were also characterized by XPS in the Ti 2p region (Fig. 5 and table 3). Based on the work of Halim et al,[49] different Ti bonds can be identified:

- a pair of asymmetric peaks corresponding to a Ti–C bond (carbide) at a binding energy of 454 eV and ~460 eV,
- a pair of peaks attributed to Ti (II) (~455 and ~461 eV),
- a pair of peaks attributed to Ti (III) (~457 and ~462 eV),
- a pair of peaks attributed to Ti (IV) (TiO_2; ~459 and 465 eV),
- a pair of peaks attributed to Ti (IV) ($TiO_{2-x}F_x$; ~460 and 466 eV), only observed on Ti_3C_2-Fe.

The first three contributions (Ti carbide, Ti^{2+} and Ti^{3+}) can be assigned to C-Ti-C in the core of the layer or C-Ti-O_x and C-Ti-$(OH)_x$ corresponding to the titanium bonded to terminal oxygen containing groups or Ti atom bonded to OH-terminations strongly physisorbed to water molecules forming Ti_3C_2OH-H_2O complexes.[49] The last two (TiO_2 and $TiO_{2-x}F_x$) are relative to the oxidation of the surface. As observed in table 3, the fraction of oxidized surface is similar for Ti_3C_2-Li and Ti_3C_2-Fe, respectively 27.8 % and 29 %, showing no major difference for the surface oxidation between the 2 MXenes. Nevertheless, the fraction of sub-oxides (Ti (II) and Ti (III)) on Ti_3C_2-Fe (60.7 %) is substantially larger than that for Ti_3C_2-Li (49.6%) and the fraction of Ti carbide is twice as small as that for Ti_3C_2-Li (10.3 % and 22.6 %, respectively) evidencing different surface reactivities of the Ti_3C_2 layers depending on the synthesis methods.

The fraction of oxidized surface obtained on our samples (~ 28 %) is higher than the fraction observed in ref 47 and 49 (~5 %) on Ti_3C_2. Our synthesis parameters (temperature and duration) are more drastic than those used in ref 47 and 49 leading probably to more oxidized surface titanium states.

Please do not adjust margins

The FeF_3/HCl etching environment has also successfully been used to prepare Ti_2CT_x MXenes from Ti_2AlC. As observed on the XRD pattern in Fig. 6, the Ti_2AlC initial MAX phase is almost completely eliminated. Contrary to Ti_3C_2-Fe, no crystallized $AlF_3.3H_2O$ is observed. The SEM micrographs in Fig. 6 confirm the formation of MXene sheets. This method can thus be generalized to the synthesis of other two-dimensional titanium carbides from aluminum-based MAX phases.

3.2 Surface functionalization

EDS measurements were performed on Ti_3C_2 MXene grains after washing in deaerated water for 1 week in order to remove impurities (mainly AlF_3) from the samples. First, the F-content decreases significantly for Ti_3C_2-HF and Ti_3C_2-Li due to the elimination of the "amorphous" AlF_3 phase observed on isolated grains whereas the Ti/F ratio of aluminum-poor Ti_3C_2-Fe isolated grain does not change significantly as expected (table 1). Secondly, the F-content is found to be higher in Ti_3C_2-HF-d (1.3 fluorine atoms per Ti_3C_2 unit formula) as compared to Ti_3C_2-Li-d (0.6 F) and Ti_3C_2-Fe-d (0.7 F) (table 1). During the synthesis process with aqueous HF, the amount of fluorine used is larger than those in the case of both other environments (initial F/Al atomic ratio = 58/1 with HF, 5/1 with LiF/HCl and 7/1 with FeF_3/HCl) which probably favors the functionalization of $Ti_3C_2T_x$ with fluorine T groups. The variation of the oxygen content determined by EDS in the samples prepared with the different etching methods is weaker (table 1). However, the interpretation of the oxygen content extracted from such measurements is not straightforward since the oxygen signal can arise from the different terminal groups (-OH, =O) of the MXene as well as from surface or interlayer water molecules. The role of water molecules is probably important since data in table 1 give a T-content close to 3 (greater than the maximum expected value of 2). Nevertheless, due to the lower amount of fluoride terminal groups, it can reasonably be considered that Ti_3C_2-Fe and Ti_3C_2-Li samples present higher amount of hydroxyl/oxygen terminal groups. At this stage, excepted for the nature of the intercalated cations, no significant difference is observed concerning the nature of terminal groups for both the LiF/HCl and the FeF_3/HCl etching methods. This change of the O/F atomic ratio as a function of the synthesis process (HF and LiF/HCl) is very consistent with recently reported results.[24,25]

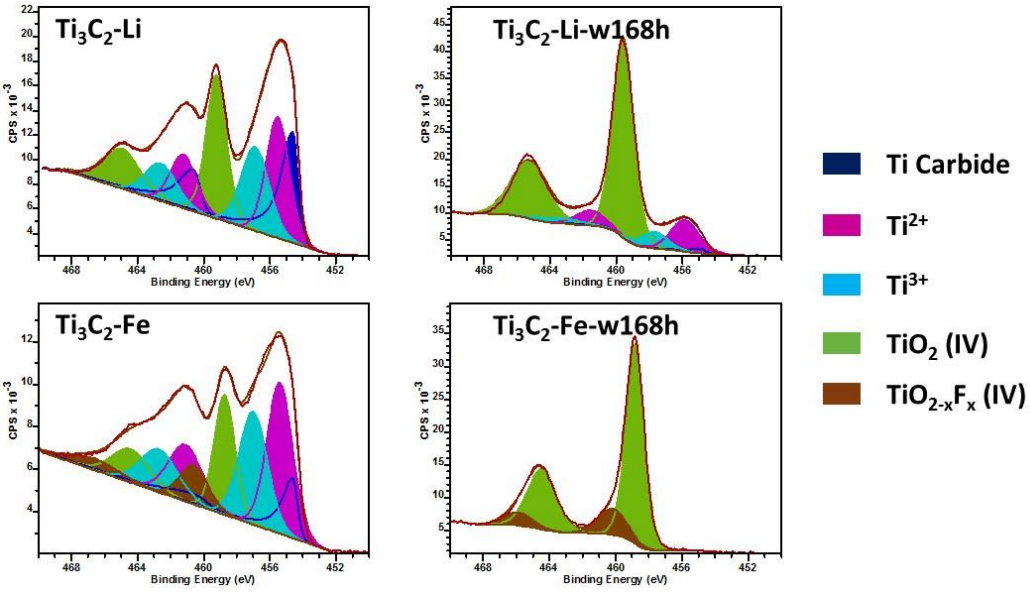

Fig. 5 XPS Ti 2p spectra recorded on (left) as-synthesized Ti_3C_2-Li and Ti_3C_2-Fe samples and (right) after the 168h immersion in water.

Table 3 XPS peak fitting results corresponding to the spectra given in Fig. 5.

	Fraction (%)			
Type of titanium in the Ti 2p region	**Ti_3C_2-Li**	**Ti_3C_2-Li-w168h**	**Ti_3C_2-Fe**	**Ti_3C_2-Fe-w168h**
Ti carbide	22.6	1.3	10.3	0
Ti^{2+}	25.3	16.8	33.3	0
Ti^{3+}	24.3	7.9	27.4	0
TiO_2 (IV)	27.8	74	20.5	90.5
$TiO_{2-x}F_x$ (IV)	0	0	8.5	9.5

This journal is © The Royal Society of Chemistry 20xx

Please do not adjust margins

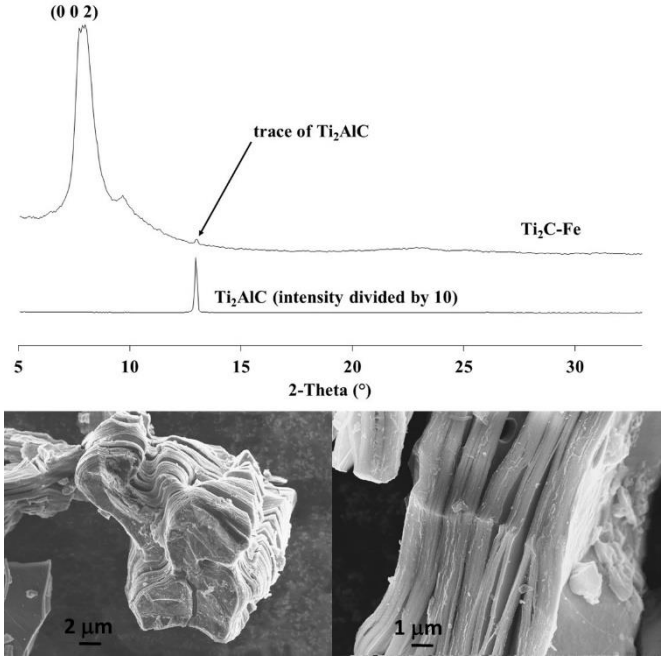

Fig. 6 XRD pattern (top) and typical SEM micrographs (down) of Ti_2C-Fe.

In order to get further insights on the surface functionalization groups, the C K- and F K-edges were recorded at the single MXene stack level using TEM-EELS. Thanks to the probe size achievable with TEM, one can be confident on the fact that the spectroscopic data are free from impurity contributions. The corresponding edges are given in Fig. 7 where a micrograph of a typical investigated stack is also given in inset, confirming again the 2D nature of the Ti_3C_2-Fe sample. The C K- and F K-edges were recently demonstrated by some of us to be powerful probes for the investigation of surface groups[25] (the notation used in Fig. 7 is thus taken from ref 25). Focusing first on the C K-edges, very little effect of the etching agent on the carbon electronic states is observed: all fine structures (from A to F) are observed at similar energy positions with very comparable relative intensities. As expected, the chemical bonds in Ti_3C_2 are weakly affected by the etching conditions. In addition, based on the analysis of the fine structures given in ref 25, we can conclude that (i) the location of the T on the MXene surface is the same for the three samples (*i.e.* pointing towards the volume titanium atoms - so-called configuration C_1) and that (ii) O-type terminations represent probably less than 20% of the surface groups in all samples (the remaining T being –F and –OH).

Moving now to the F K-edges, the spectra are also quite similar with three main fine structures labeled A to C (following the notations of ref 25) at very similar energy positions. A closer look to the fine structure C on the F K-edge of the Ti_3C_2-Fe sample evidences two weak extra peaks, labeled C_1 and C_2 which are not observed on the Ti_3C_2-Li and Ti_3C_2-HF samples. These peaks are highlighted in the inset of Fig. 7b where the spectra of the Ti_3C_2-HF and Ti_3C_2-Fe samples are superimposed (given its high noise level, the spectrum recorded on the Ti_3C_2-Li is not represented for the sake of clarity). Interestingly these two extra peaks appear at the energies of the Fe $L_{2,3}$ edge: this is consistent with the presence of iron atoms within the MXene stack in the Ti_3C_2-Fe sample. The fact that the second peak (C_2) is less intense than the first one (C_1) is also consistent with the branching ratio at the Fe $L_{2,3}$ edge. These spectra thus confirm the functionalization of the MXene sheets. The low intensity of the Fe $L_{2,3}$ edge, superimposed to the F K-edge, is consistent with the low iron content as determined from ICP and EDS measurements.

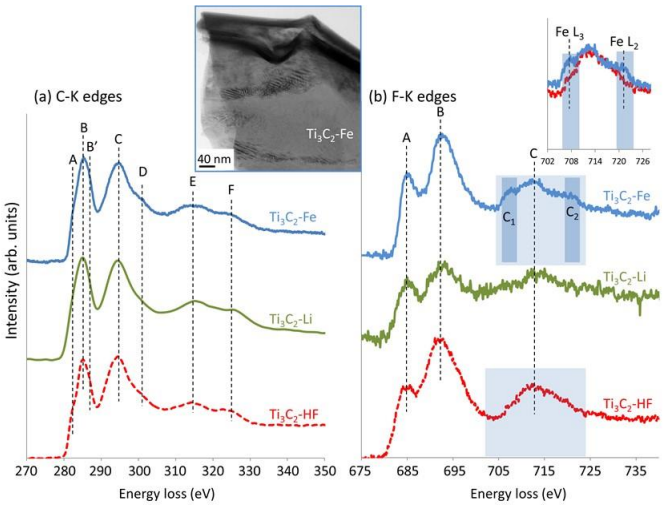

Fig. 7 (a) C K-edges recorded on the different Ti_3C_2 samples. Inset: TEM micrograph of a typical investigated stack. (b) F K-edges recorded on the different Ti_3C_2 samples. Inset: enlargement of the blue shaded areas. Spectra were aligned at the theoretical energy positions of the C K- and F K-edges (283.8 eV and 685.4 eV respectively), were normalized to their main peak intensity and were shifted vertically for the comparison. Lines are given as guides to the eyes.

3.3 Reactivity of Ti_3C_2-M with water

The three etching methods clearly lead to different compositions and/or nature of the intercalated species: different properties are thus expected. Owing to the crucial role of water for various MXenes applications, we focus on the reactivity of Ti_3C_2-M towards this medium and particularly with the aim to control selectively the oxidation process towards anatase or rutile-based TiO_2@MXenes nanocomposites.

Although the Ti_3C_2-M are stable in dearated water as observed by XRD (see Fig S2 – section III of ESI), such medium allowing the removal of impurities (AlF_3, $TiOF_2$), broad diffraction peaks of TiO_2 anatase and/or rutile are observed on sample washed in deionized water with their intensity increasing with the duration of the washing step (Fig. S2 and section III of the ESI). This oxidation of the MXenes is due to oxygen dissolved in water. However, as expected from the different roles played by Li^+ and Fe^{n+} on the AR-T, the Li or Fe-based samples behave differently. For Ti_3C_2-Li, the treatment for 168 h in water results essentially in the formation of the rutile form of TiO_2 (Fig. S2). Concerning Ti_3C_2-Fe, the formation of TiO_2 anatase is clearly evidenced after the same treatment, although a minor formation of

Please do not adjust margins

rutile is possible (Fig. S2): the selectivity towards the anatase form of TiO_2 is thus promoted compared to Ti_3C_2-Li.

The XRD (002) reflection peaks of the Ti_3C_2-Fe-w168h and Ti_3C_2-Li-w168h MXenes are shown in Fig S3. Due to the potential preferential orientation and interstratification phenomenon as discussed above, the quantification of MXene from XRD peaks is difficult. Nevertheless, the much lower intensity of the (002) peak in Ti_3C_2-Fe-w168h in comparison to the peak of Ti_3C_2-Li-w168h recorded in the same conditions indicates a higher oxidation rate after immersion in water for the MXene prepared with FeF_3/HCl etching method. This point will be confirmed by Raman and XPS spectroscopy below.

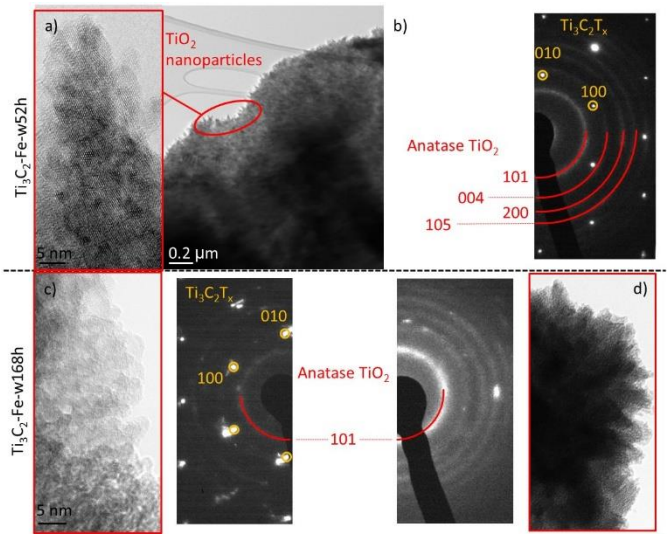

Fig. 8 (a) TEM micrographs of the Ti_3C_2-Fe-w52h sample evidencing the crystalized nanoparticles (left) covering the MXene sheets (right). (b) Corresponding energy-filtered SAED pattern (the contrast have been enhanced in order to clearly evidence the anatase rings). TEM micrographs and related SAEDP recorded on the Ti_3C_2-Fe-w168h sample and corresponding to a partially (c) and completely (d) oxidized region.

The promotion of the oxidation process towards the formation of TiO_2 anatase or rutile phases is confirmed at a local scale using transmission electron microscopy (TEM). Fig. 8a clearly evidences that for the Ti_3C_2-Fe-w52h sample, anatase nanoparticles decorate the MXene surface. The coexistence of the anatase nanoparticles and Ti_3C_2 is confirmed by the energy-filtered selected area electron diffraction pattern in Fig. 8b where the spots correspond to the MXenes structure and the rings correspond to the anatase intereticular distances. As evidenced in Fig. 8-a, the anatase nanoparticles are typically 5 nm large. The oxidation products do not change significantly with time since the same sample oxidized for one week displays also anatase nanoparticles of similar sizes (as evidenced in Fig. 8c) even in a completely oxidized region (see Fig 8d where the rings correspond to the anatase nanoparticles). Nevertheless, many more oxidized regions are observed on the sample after one week than after 52 h attesting the increase of the oxidation rate with the duration of immersion in water as confirmed by Raman spectroscopy below. The specific surface area is also increased from 10 $m^2\ g^{-1}$ for Ti_3C_2-Fe-d to 64 $m^2\ g^{-1}$ for Ti_3C_2-Fe-w168h due probably to the formation of TiO_2 nanoparticles (table 2). Even if the determination of oxygen content by EDS is controversial as discussed earlier in the text, the Ti/O atomic ratio determined by EDS confirms this oxidation since this ratio changes from 3/2.1 for Ti_3C_2-Fe to 3/5.4 for Ti_3C_2-Fe-w168h whereas the Ti/F ratio is not modified (0.7 to 0.8 F for 3 Ti). The oxidation is confirmed by SEM on Ti_3C_2-Fe-w168h since the formation of nanoparticles are clearly evidenced (Fig. 9a).

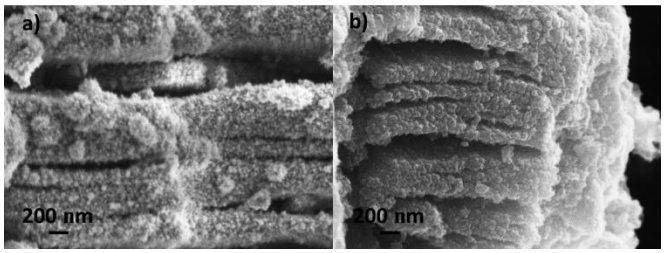

Fig. 9 Typical SEM micrographs of a) Ti_3C_2- Fe-w168h and b) Ti_3C_2-Li-w168h.

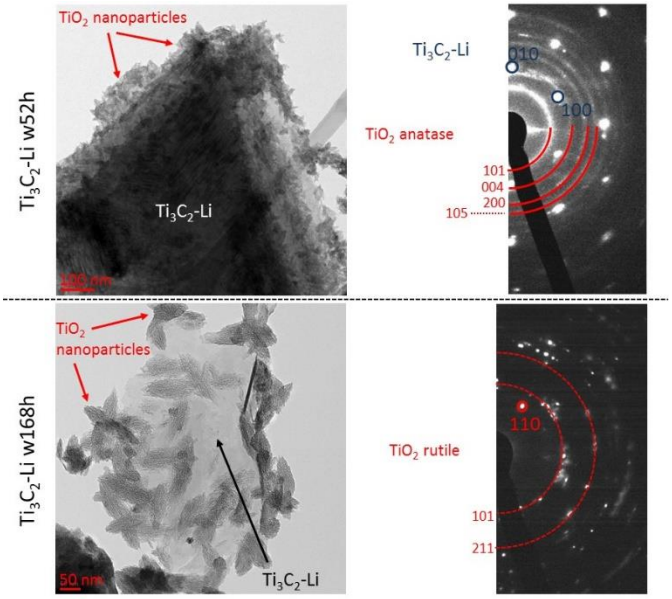

Fig. 10 Typical energy-filtered TEM micrographs and selected area electron diffraction patterns of the (top) Ti_3C_2-Li-w52h and (bottom) Ti_3C_2-Li-w168h. The SAEDP of the Ti_3C_2-w168h has been recorded on an area containing TiO_2 nanoparticles only.

The energy-filtered TEM micrographs and selected area electron diffraction patterns (SAEDP) corresponding to the Ti_3C_2-Li samples oxidized for 52h and 168h are given in the top and bottom parts of Fig. 10, respectively. The results presented confirm the decoration of $Ti_3C_2T_x$ with TiO_2 nanoparticles for every washing steps. However, for 52h treatment, the nanoparticles are mainly of anatase structure and very small (~5 to 10 nm) giving rise to rings in the SAEDP. On the contrary, the nanoparticles formed after treatment of 168h are larger (several tenths of nm), leading to a sharper peak in the XRD pattern (Fig. S2) and giving rise to spots on the SAEDP which correspond to the rutile structure of TiO_2. These results evidence the transformation of the nanoparticles from anatase to rutile while growing. As in the case of Ti_3C_2-Fe, the specific surface area and the

This journal is © The Royal Society of Chemistry 20xx

Please do not adjust margins

Please do not adjust margins

Ti/O ratio increase (table 2), and nanoparticles are observed by SEM (Fig. 9b) confirming the surface oxidation process. Finally, one can notice that the Ti/F ratio does not change significantly in water with time (table 2).

Raman spectra of Ti_3C_2-Fe and Ti_3C_2-Li after water treatment are presented in Fig. 11. After immersion of Ti_3C_2-Fe and Ti_3C_2-Li in deaerated water (labelled Ti_3C_2-Fe-d and Ti_3C_2-Li-d respectively), the characteristic peaks of $Ti_3C_2T_X$ are still present: the deaerated treatment has no significant effect on the MXenes oxidation in agreement with the XRD patterns. After immersion in deionized water for 168h, new peaks at 158 cm^{-1}, 419 cm^{-1}, 507 cm^{-1} and 620 cm^{-1} are detected for Ti_3C_2-Fe-w168h. The peaks at 158 cm^{-1} and 507 cm^{-1} can be attributed to the $E_{g(1)}$ and A_{1g} vibrational modes of TiO_2 anatase respectively. The peak at 419 cm^{-1} can be interpreted as the superposition of the E_g vibrational mode of TiO_2 rutile with the A_{1g} mode of TiO_2 anatase and the peak at 620 cm^{-1} to the superposition of the A_{1g} mode of TiO_2 rutile and the $E_{g(3)}$ mode of TiO_2 anatase. Thus, the presence of rutile cannot be totally excluded. The Raman signature of $Ti_3C_2T_X$ is only detected through the shoulder at 208 cm^{-1} and 576 cm^{-1} attesting the high oxidation rate on this sample, in agreement with XRD results. On the contrary, the Raman spectra of Ti_3C_2-Li-w168h is similar to Ti_3C_2-Li. The absence of a peak corresponding to TiO_2 anatase at 158 cm^{-1}, i.e. the most intense vibration mode, indicates that this phase is not formed, in agreement with previous XRD results. Concerning the TiO_2 rutile phase, its vibration frequencies close to that of $Ti_3C_2T_x$ does not allow to confirm or invalidate the presence of this phase. But, for the same immersion time in deionized water Ti_3C_2-Fe is clearly more oxidized than the Ti_3C_2-Li.

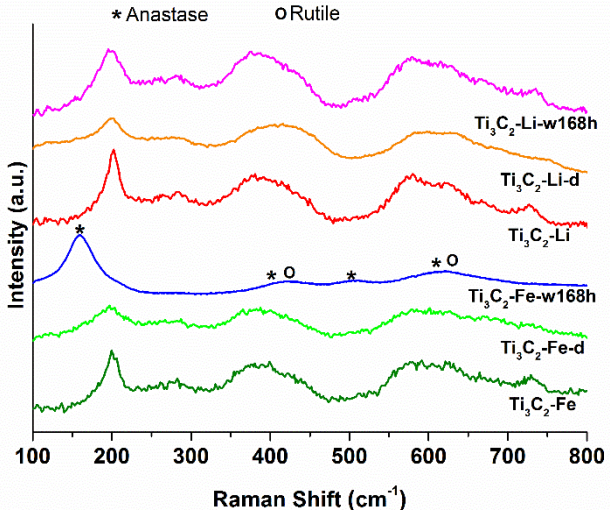

Fig.11 Raman spectra of Ti_3C_2-Fe and Ti_3C_2-Li after water treatment

XPS analyses (table 2 and Fig. 5) clearly evidenced the oxidation of the MXene surfaces after 168h in deionized water, with the important increase of the fraction corresponding to TiO_2 compared to the initial MXene phases (Ti_3C_2-Li and Ti_3C_2-Fe). As observed by Raman spectroscopy and XRD, the oxidation is more important in the case of Ti_3C_2-Fe-w168h compared to Ti_3C_2-Li-w168h since the Ti (IV) fraction is 100 % showing that the surface of this MXene is totally oxidized (Ti (IV) fraction = 74 % for Ti_3C_2-Li-w168h). The larger amount of oxygen measured by EDS (Ti/O of 3/5.4 for Ti_3C_2-Fe-w168h and 3/4.5 for Ti_3C_2-Li-w168h) is in agreement with the higher oxidation rate in the case of iron containing etching agent. Moreover, the larger specific surface area of Ti_3C_2-Fe-w168h (64 m^2 g^{-1}) compared to that obtained with Ti_3C_2-Li-w168h (27 m^2 g^{-1}) is also consistent with this result (higher amount of Nps).

The Ti_3C_2-Fe oxidation rate can be controlled by the immersion time in water allowing to optimize the TiO_2@MXene composite composition. As observed on the Raman spectra (Fig. S7 –section VII of the ESI), the intensity of the spectral signature of TiO_2 anatase increases with the duration of immersion while the spectral signature of the MXene decreases in agreement with the XRD data reported on the same figure showing the increase of the TiO_2 peaks intensity with time.

The origin of the different behaviors towards the oxidation into water between the MXenes prepared by LiF/HCl and FeF_3/HCl (higher rate of oxidation and promotion of anatase in Ti_3C_2-Fe) is probably multifactorial. In order to evidence the role of the cations/salts on the AR-T, different procedures have been developed in order to selectively remove the Fe^{n+} and Al^{3+} from the Ti_3C_2-Fe samples before the oxidation tests:

- Fe^{n+} cations can be selectively removed (as evidenced by the ICP-OES quantifications given the table S1 of the ESI – section VI) by centrifugation in 6M HCl (3 times) and deionized water (3 times) before filtration. This step does not remove Al and the corresponding samples are labelled Ti_3C_2-Fe-HCl (see section VI of ESI for a deeper discussion).
- Al^{3+} cations can be selectively removed (see section VI and table S1 of ESI) by a simple washing step in deaerated water for 5h at low concentration (0.6 g of powder for 350 ml of water). The corresponding samples are labelled Ti_3C_2-Fe-d5h.
- The combination of the two steps leads to the removal of both Fe and Al cations (table S1). The corresponding samples are labelled Ti_3C_2-Fe-HCl-d5h.

As evidenced by the XRD patterns in Fig. 12, the removal of Al or Fe favors the AR-T as shown by the evolution of the relative intensity of diffraction peaks of the rutile and anatase phases. A synergy effect is evidenced since the rutile contribution to the XRD pattern is significantly increased when both cations are removed. Nevertheless, anatase TiO_2 is still observed on each sample (this is confirmed by Raman spectroscopy measurments as discussed section VI of ESI). Such behaviour is consistent with the fact that the first oxidation steps probably involves very small Nps which are transformed into rutile while growing. On the contrary, similar washing steps performed on Ti_3C_2-Li always leads to rutile after 168h. This observation can be ascribed to the fact that Li^+ is a promoter of the AR-T together with the fact that rutile is the stable polymorph structure after the Np growth. One can notice that the addition of Al^{3+} ions in water, through the dissolution of AlF_3 with a similar Ti/Al ratio as that obtained for Ti_3C_2-Fe, for the treatment of Ti_3C_2-Li (see section VI of ESI for more details) is not enough to modify this trend: the sample oxidation always results in the formation of a majority of rutile after 168h. In addition, the MXene oxidation rate can also play a role on the anatase/rutile selectivity: the higher the oxidation rate, the higher the formation of the anatase fraction.

This journal is © The Royal Society of Chemistry 20xx

Please do not adjust margins

Please do not adjust margins

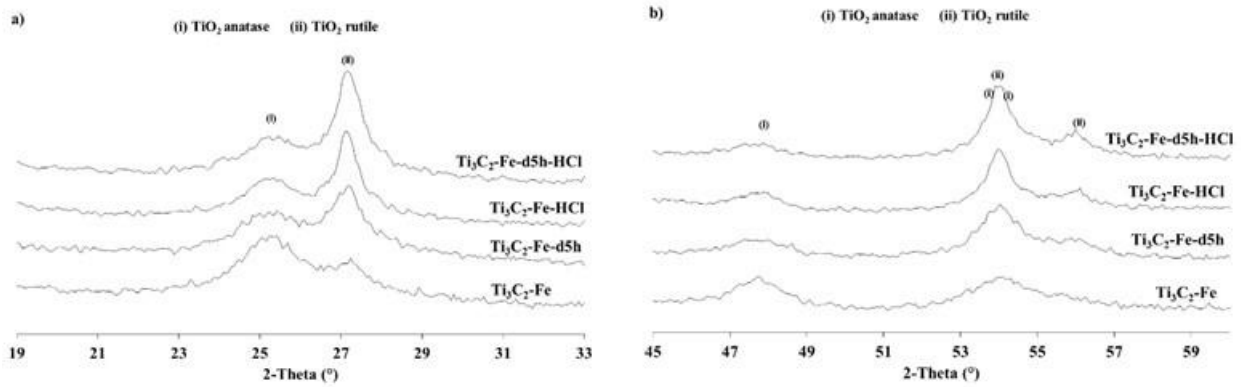

Fig. 12 XRD patterns after washing into deionized water of different MXene prepared from FeF_3/HCl.

The higher oxidation rate observed with the FeF_3/HCl etching method can be explained using XPS results. As discussed previously (section 3.1), after synthesis, the fraction of Ti(II) and Ti(III) at the surface for the MXene prepared by FeF_3/HCl is higher whereas the fraction of Ti carbide is lower compared to Ti_3C_2-Li. During the etching process, Fe^{3+} cations probably oxidize partially the surface titanium ($Ti^{n+} \rightarrow Ti^{(n+1)+}$) during the exfoliation of aluminum, thus weakening the surface and favoring the oxidation phenomenon after immersion in water. This oxidizing ability of Fe^{3+} on the MXene is confirmed on all samples since, whatever the initial etching method, they are totally oxidized after treatment with a $FeCl_3$ solution.

The oxidation of Ti_3C_2 in water has already been reported[47] and the positive effect of TiO_2@Ti_3C_2 on the photocatalytic activity has been evidenced[15] and confirmed later.[36,50] Such hybrid structures take advantage of the MXene electronic conductivity to reduce recombination effects through electrons transport. Considering that anatase structure displays higher photocatalytic activity than rutile structure,[51] the synthesis method proposed here, which allows the partial inhibition of the AR-T and a control of the oxidation rate is very convenient for enhanced photocatalytic properties of oxidized Ti_3C_2. Such promising properties exceed photocatalytic applications as recently demonstrated for Li-ion battery electrodes[52], supercapacitors[35] or environmental remediation.[53]

4 Conclusion

In summary, we propose a new, cheap and safe etching environment (FeF_3/HCl mixture) for the synthesis of two-dimensional titanium carbides from the corresponding MAX phase precursors, thereby expanding the preparation methods for this promising family of 2D materials while offering new opportunities for their surface functionalization.

Comparison to the conventional HF etching method, the Ti_3C_2 obtained with FeF_3/HCl exhibits lower fluorine content and no secondary phase like $TiOF_2$ while allowing simultaneously the intercalation of iron cations between the MXene layers. Such modifications of the MXenes surface functionalization lead to significant changes in their hydrophilic properties: water intercalation between the MXene sheets is obtained, leading to the formation of a material with various c parameters depending on the drying process as in the case of the LiF/HCl etching method. The penetration of water is a key element for catalytic and electrocatalytic applications such as fuel cells where the water diffusion plays a crucial role. Further investigation of these iron intercalated MXenes in catalysis or in metal-ion capacitors may be an attractive prospect.[4]

Combining state of the art characterizations, allowing local and surface sensitive investigations, of the LiF/HCl and FeF_3/HCl etching methods for the production of Ti_3C_2 evidences a considerably modified reactivity vs water when changing the etching agent. Although the oxidation in water, leading to the decoration of the MXene with TiO_2 nanoparticles, is observed independently on the synthesis process (this oxidation can be avoided in deaerated water), the selectively towards the formation of anatase, which is crucial in photocatalysis for instance, is however promoted using the FeF_3/HCl etching environment whereas the rutile form is favored with LiF/HCl. In addition, the oxidation rate of the FeF_3/HCl samples, which is greater than that of the LiF/HCl samples, can be controlled with the duration of immersion in water, leading to the formation of various ratios of TiO_2/Ti_3C_2. Such a combination of the control of both the AR-T and the oxidation rate gives great flexibility in the design of TiO_2@Ti_3C_2 nanocomposites.

The inhibition or promotion of the anatase to rutile transformation is multifactorial, one key element being the nature of the intercalated cations and salts impurities, highlighting the need for etching environments which simultaneously allow optimized surface functionalization. This point is all the more important that the here proposed etching method can probably be generalized to many other transition metal salts (e.g. CoF_2) offering many other opportunities for the MXene functionalization. The oxidation rate is also possibly involved in the above mentioned selectivity. The different oxidation rates for equivalent treatments in water are attributed to the different surface chemistry of the MXene depending on the etching environment. Indeed, more oxidized titanium being observed on the MXene surface prepared from FeF_3/HCl method (probably due to the partial oxidation of titanium by Fe^{3+} during the etching) favoring the oxidation after immersion in water.

These results provide a simple alternative to the thermal treatments[46,52,54] or chemical processes[35-37,50,53] for the controlled

Please do not adjust margins

Please do not adjust margins

oxidation of MXenes, and offer new opportunities for various applications including photocatalysis and electrocatalysis applications.

Whereas the promising future of this 2D family has been already established, partly based on the large range of potential compositions due to the richness of the parent family (MAX phases), this work pushes further our understanding of the crucial role of the etching environment on the MXene surface chemistry and gives new opportunities to improve the exciting properties of these materials for several applications.

5 Acknowledgements

The authors wish to thanks Nadia Guignard for Raman spectroscopy, Christine Canaff for XPS and Lilian Eloy for ICP-OES, and the fruitful discussion about the data. Poitiers University is gratefully acknowledged for financial support through ATI project ("Action Transversale Incitative" 2015). This work partially pertains to the French Government program "Investissements d'Avenir" (LABEX INTERACTIFS, reference ANR-11-LABX-0017-01). D.M. thanks the "Région Poitou-Charentes" for financial support. The "Agence Nationale de la Recherche" is gratefully acknowledged for financial support: ANR project no. 13-BS090024-02.

References

1 M.Naguib, M. Kurtoglu, V. Presser, J. Lu, J. Niu , M. Heon , L. Hultman , Y. Gogotsi and M. W. Barsoum, *Adv. Mater.* 2011, **23**, 4248–4253
2 M. Naguib, O. Mashtalir, J. Carle, V. Presser, J. Lu, L. Hultman, Y. Gogotsi and M. W. Barsoum, *ACS Nano*, 2012, **6**, 1322–1331
3 M. W. Barsoum, *MAX Phases: Properties of Machinable Ternary Carbides and Nitrides*, John Wiley & Sons, 2013
4 M. R. Lukatskaya, O. Mashtalir, C. E. Ren, Y. Dall'Agnese, P. Rozier, P. L. Taberna, M. Naguib, P. Simon, M. W. Barsoum and Y. Gogotsi, *Science,* 2013, **341**, 1502–1505
5 Z. Lin, B. Daffos, P-L. Taberna, K. L. Van Aken, B. Anasori, Y. Gogotsi and P. Simon, *J. Power Sources*, 2016, **326**, 575–579
6 M. Naguib, J. Come, B. Dyatkin, V. Presser, P-L. Taberna, P. Simon, M. W. Barsoum and Y. Gogotsi, *Electrochem. Commun*., 2012, **16**, 61–64
7 M. Naguib, J. Halim, J. Lu, K. M. Cook, L. Hultman, Y. Gogotsi and M. W. Barsoum, *J. Am. Chem. Soc.*, 2013, **135**, 15966−15969
8 Y. Xie, Y. Dall'Agnese, M. Naguib, Y. Gogotsi, M. W. Barsoum, H. L. Zhuang and P. R. C. Kent, *ACS Nano*, 2014, **8**, 9606–9615
9 X. Xie, S. Chen, W. Ding, Y. Nie and Z. Wei, *Chem.Commun.*, 2013, **49**, 10112−10114
10 Z. Guo, J. Zhou, L. Zhua and Z. Sun, *J. Mater. Chem. A*, 2016, **4**, 11446–11452
11 X. Zhang, J. Lei, D. Wu, X. Zhao, Y. Jing and Z. Zhou, *J. Mater. Chem. A*, 2016, **4**, 4871–4876
12 Y. Gao, L. Wang, Z. Li, A. Zhou, Q. Hu, X. Cao, *Solid State Sci.*, 2014, **35**, 62–65
13 H. Qianku, S. Dandan, W. Qinghua, W. Haiyan,W. Libo, L. Baozhong, Z. Aiguo and H. Julong, *J. Phys. Chem. A*, 2013, **117**, 14253–14260
14 W. Fen, Y. Chen Hui, D. C. Yue, X. Dan; T. Yi and Z. Jian Feng, *J. Electrochem. Soc*., 2015, **162**, B16–B21
15 O. Mashtalir, K. M. Cook, V. N. Mochalin, M. Crowe, M. W. Barsoum and Y. Gogotsi, *J. Mater. Chem. A,* 2014, **2**, 14334–14338
16 D. Magne, V. Mauchamp, S. Célérier, P. Chartier and T. Cabioc'h, *Phys. Rev. B,* 2015, **91**, 201409
17 C. E. Ren, K. B. Hatzell, M. Alhabeb, Z. Ling, K. A. Mahmoud and Y. Gogotsi, *J. Phys. Chem. Lett*., 2015, **6**, 4026−4031
18 Y. Xue-fang, L. Yan-chun, C. Jian-bo, L. Zhen-bo, L. Qing-zhong, L. Wen-zuo, Y. Xin, X. Bo, *ACS Appl. Mater. Interfaces,* 2015, **7**, 13707–13713
19 Q. Peng, J. Guo, Q. Zhang, J. Xiang, B. Liu, A. Zhou, R. Liu and Y. Tian, *J.Am.Chem.Soc*., 2014, **136**, 4113–4116
20 M. Naguib, V. N. Mochalin, M. W. Barsoum and Y. Gogotsi, *Adv.Mater*., 2014, **26**, 992–1005
21 J-C. Lei, X. Zhang and Zhen Zhou, *Front. Phys.*, 2015, **10**, 276–286
22 B. Anasori, M. R. Lukatskaya and Y. Gogotsi, *Nature Rev.*, 2017, 16098
23 V. M. H. Ng, H. Huang, K. Zhou, P. S. Lee, W. Que, J. Z. Xu and L. B. Kong, *J. Mater. Chem. A,* 2017, **5**, 3039–3068
24 H-W. Wang, M. Naguib, K. Page, D. J. Wesolowski and Y. Gogotsi, *Chem. Mater.*, 2016, **28**, 349–359
25 D. Magne, V. Mauchamp, S. Célérier, P. Chartier and T. Cabioc'h, *Phys. Chem. Chem. Phys.,* 2016, **18**, 30946–30953
26 Y. Xie, M. Naguib, V. N. Mochalin, M. W. Barsoum, Y. Gogotsi, X. Yu, K-W. Nam, X-Q. Yang, A. I. Kolesnikov and P. R. C. Kent, *J. Am. Chem. Soc.*, 2014**, 136,** 6385–6394
27 M. Khazaei, M. Arai, T. Sasaki, C-Y. Chung, N. S. Venkataramanan, M. Estili, Y. Sakka and Y. Kawazoe*, Adv. Funct. Mater.,* 2013, **23**, 2185–2192
28 V. Mauchamp, M. Bugnet, E.P. Bellido, G.A. Botton, P. Moreau, D. Magne, M. Naguib, T. Cabioc'h and M.W. Barsoum, *Phys. Rev. B*, 2014, **89**, 235428
29 S. Lai, J. Jeon, S. K. Jang, J. Xu, Y. J. Choi, J-H. Park, E. Hwang and S. Lee, *Nanoscale*, 2015, **7**, 19390–19396
30 J. Halim, M. R. Lukatskaya, K. M. Cook, J. Lu, C. Smith, L-Å. Näslund, S. J. May, L. Hultman, Y. Gogotsi, P. Eklund and M. W. Barsoum, *Chem. Mater.*, 2014, **26**, 2374–2381
31 M. Ghidiu, M. R. Lukatskaya, M-Q. Zhao, Y. Gogotsi and Michel W. Barsoum, *Nature*, 2014, **516**, 78–81
32 M. Ghidiu, J. Halim, S. Kota, D. Bish, Y. Gogotsi and M. W. Barsoum, *Chem. Mater.*, 2016, **28**, 3507–3514
33 F. Liu, A. Zhoua, J. Chena, J. Jia, W. Zhou, L. Wang, Q. Hu, *Appl. Surf. Sci.*, 2017, **416**, 781–789
34 B. Ahmed, D. H. Anjum, M. N. Hedhili, Y. Gogotsi and H. N. Alshareef, *Nanoscale,* 2016, **8**, 7580–7587
35 J. Zhu,a, Y. Tang, C. Yang, F. Wang and M. Caoa, *J. Electrochem. Soc.*, 2016, **163**, A785–A791
36 C. Peng, X. Yang, Y. Li, H. Yu, H. Wang and F. Peng, *ACS Appl. Mater. Interfaces,* 2016, **8**, 6051−6060
37 F. Wang, C. Yang, M. Duan, Y. Tang and J. F. Zhu, *Biosens. Bioelectron.,* 2015, **74**, 1022–1028
38 H. Zhang and J. F. Banfield, J. Mater. Chem. 1998, **8**, 2073-2076
39 D. A. H. Hanaor and C. C. Sorrell, *J. Mater. Sci.*, 2011, **46**, 855−874
40 Q. Gao, X. Wu and Y. Fan, *Dyes and Pigments*, 2012, **95**, 96–101
41 J. B. Goodenough and K. S. Park, *J. Am. Chem. Soc.,* 2013, **135**, 1167–1176
42 R.F. Egerton, *Electron energy-loss spectroscopy in the electron microscope,* Plenum Press, New York, 1996.
43 O. Mashtalir, M. Naguib, B. Dyatkin, Y. Gogotsi, M. W. Barsoum, Mater. Chem. Phys., 2013, **139**, 147–152
44 E. Ferrage, B. Lanson, L. J. Michot and J-L. Robert, *J. Phys. Chem. C,* 2010, **114**, 4515–4526

Please do not adjust margins

Please do not adjust margins

45 N. C. Osti, M. Naguib, A. Ostadhossein, Y. Xie, P.R. C. Kent, B. Dyatkin, G. Rother, W. T. Heller, A. C. T. van Duin, Y. Gogotsi and E. Mamontov, *ACS Appl. Mater. Interfaces*, 2016, **8**, 8859–8863
46 M. Naguib, O. Mashtalir, M. R. Lukatskaya, B. Dyatkin, C. Zhang, V. Presser, Y.Gogotsi and M. W. Barsoum, *Chem. Commun*.**,** 2014, **50**, 7420–7423
47 C. J. Zhang, S. Pinilla, N. McEvoy, C. P. Cullen, B. Anasori, E. Long, S-H. Park, A. Seral-Ascaso, A. Shmeliov, D. Krishnan, C. Morant, X. Liu, G. S. Duesberg, Y. Gogotsi and V. Nicolosi, *Chem. Mater.*, 2017, **29**, 4848–4856
48 T. Hu, J. Wang, H. Zhang, Z. Li, M. Huab and X. Wang, *Phys. Chem. Chem. Phys.*, 2015, **17**, 9997–10003
49 J. Halim, K. M. Cook, M. Naguib, P. Eklund, Y. Gogotsi, J. Rosen, M. W. Barsoum, *Appl. Surf. Sci.*, 2016, **362**, 406–417
50 Y. Gao, L. Wang, A. Zhou, Z. Li, J. Chen, H. Bala, Q. Hu and X. Cao, *Mater. Lett*., 2015, **150**, 62–64
51 T. Luttrell, S. Halpegamage, J. Tao, A. Kramer, E. Sutter and M. Batzill, *Sci. Rep.,* 2014, **4**, 4043
52 C. J. Zhang, S. J. Kim, M. Ghidiu, M-Q. Zhao, M. W. Barsoum, V. Nicolosi and Y. Gogotsi, *Adv. Funct. Mater.*, 2016, **26**, 4143–4151
53 G.Zou, J. Guo, Q. Peng, A. Zhou, Q. Zhang and B. Liu, *J. Mater. Chem. A*, 2016, **4**, 489–499
54 H. Ghassemi, W. Harlow, O. Mashtalir, M. Beidaghi, M. R. Lukatskaya, Y. Gogotsi and M. L. Taheri, *J. Mater. Chem. A*, 2014, **2**, 14339–14343

This journal is © The Royal Society of Chemistry 20xx

Please do not adjust margins